

Direct Observation and Analysis of Annealing-Induced Microstructure at Interface and Its Effect on Performance Improvement of Organic Thin Film Transistors

Qiaoliang Bao,^{†,§} Jun Li,^{†,§} Chang Ming Li,^{*,†} Zhi Li Dong,[‡] Zhisong Lu,[†] Fang Qin,[†] Cheng Gong,[†] and Jun Guo[†]

School of Chemical and Biomedical Engineering and Center for Advanced Bionanosystems, Nanyang Technological University, Singapore, 639798, Singapore, and School of Materials Science and Engineering, Nanyang Technological University, Nanyang Avenue, Singapore 639798, Singapore

Received: June 5, 2008; Revised Manuscript Received: August 2, 2008

For the first time direct observation and analysis of microstructural variations of crystalline domains and grain boundaries at atomic scale in the buried interface of an organic semiconductor thin film of poly(2,6-bis(3-alkylthiophen-2-yl)dithieno[3,2-*b*;2',3'-*d*]thiophene) (PBTDT), a new synthesized solution-processed polymer is achieved for demonstrating a different network nanostructure of crystalline nanofibers at the interface from the outside surface of the film observed. It is also discovered that structural variations of crystalline domains and grain boundaries at an atomic scale caused by annealing, which include larger domains with enhanced crystallinity, reduced $\pi-\pi$ stacking distance, reduced disorders in the grain boundaries, and small tilt-angle boundaries well explain the significant performance improvement of the PBTDT based organic thin film transistor (OTFT) after annealing. This work provides a highly resolutioned image on the microstructures at an organic semiconducting interface for deep scientific insights of the OTFT performance improvement through microstructure optimization.

1. Introduction

Semiconducting polymers have been intensively investigated to fabricate light-emitting diodes,^{1–3} photovoltaic cells,^{4,5} and thin film field-effect transistors,^{6–12} of which organic thin-film transistors (OTFTs) are in particular scientifically and technically interesting due to their broad applications in flexible and large-area electronic circuits.^{9,13} The main challenge for OTFT practical applications is to improve their charge carrier mobility close to amorphous silicon by designing novel chemical structure and optimizing fabrication processes. The charge carrier mobility is crucially dependent on the structural order of the semiconductor molecules, since band transport within an ordered lamella of microcrystalline domains is much more efficient than intermolecular charge hopping across grain boundaries or through disordered domains.^{14,15} A number of process approaches such as controlled solvent evaporation,^{16,17} appropriate chemical treatment of substrate surface^{18,19} and thermal post-treatment (annealing)^{20,21} have been developed to enhance molecular ordering of solution-deposited OTFTs. These efforts directly leads to great research interests to explore scientific insights of the relationship of charge-transport/injection physics of organic semiconductors and their microstructure–property, particularly at the interface of organic semiconductor/dielectric layer.⁸

However, the critical microstructure responsible for the charge-transport in an OTFT is buried in the semiconductor/dielectric interface of approximately 5 nm from the semiconductor surface.²² Up to date, the buried interface is not

readily accessible with conventional structural characterization methods for investigation.²³ Generally, atomic force microscopy (AFM) can characterize the exposed outside surface morphology of the thin film on a bottom-gate-structured OTFT and assume an identical microstructure existed in the whole interface layer.^{22,24–29} The unclear microstructure and conformation at the buried interface may cause confusion and controversy on the mechanism responsible for improved transistor performance, particularly the effects of electrode surface modification and annealing. It is of importance for direct observation and analysis of the microstructure at the buried interface of the organic semiconductor thin film contacted with the dielectric layer.

The crystalline structure of the organic semiconductor thin film is often studied by X-ray diffraction (XRD)^{10,30} or grazing-incidence XRD (GIXRD),^{12,31,32} of which the results only represent an average structure over a bulk material, and might not identify different phase components or much finer structural characteristics. Most recently, the buried interfaces in a OTFT are studied by using vibrational spectroscopy,^{33,34} high-energy X-ray beam,³⁵ near-edge X-ray absorption spectroscopy (NEXAFS)^{36–38} and rocking curves.³⁹ However, these techniques suffer from poor spatial resolution to distinguish crystalline from amorphous. It is a great challenge to directly image the buried interface by using a high resolution microscopy for observation and analysis of the microstructure for detail crystallinity and orientation within domains and boundaries, then providing better understanding of the structure–property relationships at an atomic scale.

In our previous work, a new solution-processable polymer poly(2,6-bis(3-alkylthiophen-2-yl)dithieno[3,2-*b*;2',3'-*d*]thiophene) (PBTDT) is synthesized to fabricate OTFTs with excellent performance (mobility of $0.3 \text{ cm}^2 \text{ V}^{-1} \text{ s}^{-1}$ and on/off ratio over 10^7) and great ambient stability particularly after annealing at 160°C for 1 h,⁴⁰ in sharp contrast to the

* To whom correspondence should be addressed. E-mail: ecmli@ntu.edu.sg. Telephone: 65-6790-4485. Fax: 65-6790-4485.

[†] School of Chemical and Biomedical Engineering, Nanyang Technological University.

[‡] School of Materials Science and Engineering, Nanyang Technological University.

[§] These authors contributed equally to this work.

performance of a mobility about $0.006 \text{ cm}^2 \text{ V}^{-1} \text{ s}^{-1}$ and a current on/off ratio about 10^3 without post thermal-treatment (See Figure S1 in the Supporting Information for transistor properties). Although the XRD pattern reported in our previous work⁴⁰ demonstrates that the annealing leads to more enhanced crystallinity, the detail variations of the microstructure, especially that in the buried interface for explain the performance enhancement of the PBTDT OTFT is not clear. In this work, a freestanding PBTDT thin film was fabricated to directly examine the microstructures in the interface before and after annealing by both AFM and high resolution transmission electron microscopy (HRTEM). Analysis of the microstructure variations after annealing was conducted to reveal the scientific insight of performance improvement of annealed OTFTs.

2. Experimental Section

PBTDT was synthesized via Stille coupling polymerization of 2,6-bis(trimethylstannanyl)dithieno[3,2-*b*;3'-*d*]thiophene with 5,5'-dibromo-4,4'-dialkyl[2,2']bithiophene, as reported in our previous work.⁴⁰ The transistor fabrication and measurements were also carried out as the method we introduced before.⁴⁰ Mica was chose as substrate to prepare thin film because it has similar surface chemistry (i.e., $-\text{OH}$ groups)⁴¹ and coefficient of thermal expansion as those of commonly used gate dielectric SiO_2 . Freshly cleaved mica with atom-scale ultra flat surface was pretreated with 0.1 M octyltrichlorosilane (OTS-8) solution for 45 min to grow a silane SAM. The modified mica was washed using toluene and isopropyl alcohol and then dried by nitrogen. 5 mg/mL PBTDT nanoparticles suspension in chlorobenzene was spin-coated onto OTS-modified mica at a speed of 2000 rpm to form a thin film less than 100 nm. Then the samples were dried in vacuum for 15 min. For post thermal treatment, the sample was annealed at 160 °C for 1 h and cooled in a vacuum overnight. The PBTDT thin films were subsequently delaminated from the mica by dipping the samples into water using a floating off process^{41–44} to obtain a freestanding film for exposure of the interface formed on the solid mica surface. The microstructures of the films were characterized with AFM and HRTEM.

For the AFM experiments, the delaminated thin films were attached onto Si wafer with the bottom surface of interface upturned. The surface morphology of the interface was characterized by AFM (SPM 3100, Veeco Instruments Inc., USA) operating in tapping mode at ambient temperature. Both topographical and phase images were acquired at the same time. For the HRTEM observation, the delaminated thin films were transferred onto 300 mesh copper grids with the interface layer exposed (see Figure S2 (Supporting Information) for optical image of the film). The microstructures were examined by using a high resolution transmission electron microscope (JEM 2100F, JEOL, Japan) with the working voltage at 200 kV. The point resolution of the HRTEM is 0.19 nm. In order to minimize the electron irradiation effect, we employed optimized parameters for imaging by reducing the exposure time and electron dose as low as possible. Before the AFM and HRTEM characterizations, samples were vacuum-dried and stored. The simulated HRTEM image was calculated by using electron microscopy software JEMS (CIME-EPFL, Switzerland) based on the multislice method⁴⁵ with $\Delta f = -43 \text{ nm}$ and $t = 20.9 \text{ nm}$.

3. Results and Discussion

3.1. AFM Morphologies.

Figure 1 illustrates the AFM morphologies of the interface of PBTDT thin film without annealing, of which the large scaled topography in Figure 1a

reveals that PBTDT nanoparticles distribute separately but homogeneously in the thin layer interface formed on a mica surface, and Figure 1b and 1c, the topography and phase signals respectively clearly present the round-shaped rod-like PBTDT nanoparticles across the entire scan area ($1.1 \times 1.1 \mu\text{m}$). The cross-section in Figure 1d taken across the particle or fibers display sizes of 25–35 nm (marked I, II, and III in Figure 1b), which is very close to that of PBTDT nanoparticles⁴⁰ in the suspension, indicating that PBTDT in the film formed from its precursor solution without heat-treatment inherits its physical properties in solution phase without significant change. The AFM morphologies of the interface layer after annealing show a network structure consisting of randomly interconnected nanofibers in Figure 2a, of which magnified topography and phase image are shown in Figure 2, parts b and c ($1.1 \times 1.1 \mu\text{m}$). The diameter of the nanofibers is about 45–60 nm determined by their cross-sections (Figure 2d), nearly two times larger than that without annealing (Figure 1d). The sizes of domains after annealing increase anisotropically to a submicron range along the prolonged dimension. This suggests that the annealing process produces significantly larger domains with lengthy fiber-like structures, possibly indicating that domains are restructured and merged at the annealing temperature.¹¹ However, these morphologies of the interface are totally different from those of outside surface and mica surface (see Figure 3 and Figure S3 (Supporting Information)), in which the outside surface of PBTDT thin film shows featureless and has no significant change except a decreased surface roughness after annealing. These discrepancies might originate from the different degree of order^{36,39} and space-restriction effects⁴¹ between the interface and the outside surface. The exposed outside surface morphology of the thin film on a bottom-gate-structured OTFT is previously studied by using AFM with an assumption of an identical microstructure in the whole thin active layer.^{22,24,25,27,28} However, for the first time our work demonstrates that the interface of the polymer thin film has morphologies and structural characteristics very distinctive from the outside surface.

It is known that the interface layer is mainly responsible for the charge transfer in a thin film transistor.²² Thus, the microstructure changes at the interface of PBTDT thin film after annealing may play the critical role in the improvement of charge mobility of the fabricated device.⁴⁰ First, the broadening of the nanocrystalline width accompanied with increased effective conjugated length (also verified by optical measurements shown in Figure S4 in Supporting Information) demonstrated in our work can exponentially enhance the charge carrier mobility in OTFTs fabricated from the well-ordered polymer PBTDT.²⁶ This is because that the transport along the conjugated segments of the polymer backbone is faster than interchain hopping between adjacent chains and the conjugated length can also provide higher possibility for charge carrier transport from one chain to another.^{46,47} Additionally, the broadening of the nanocrystalline in the film can decrease the hopping process between domains to improve the charge carrier mobility. These results agree well with recent works that report mobility of π -conjugated polymers can be further improved by increasing their molecular weight and choosing appropriate deposition methods to form nanofibers or nanowires structure.^{22,24–27} Second, the better connectivity of neighboring nanofibers in the interface layer would be expected to make interfiber charge transport easier by increasing the electronic overlap between neighboring nanofibers,⁴⁸ and then improve mobilities, while the charge transport in unannealed film is limited by the

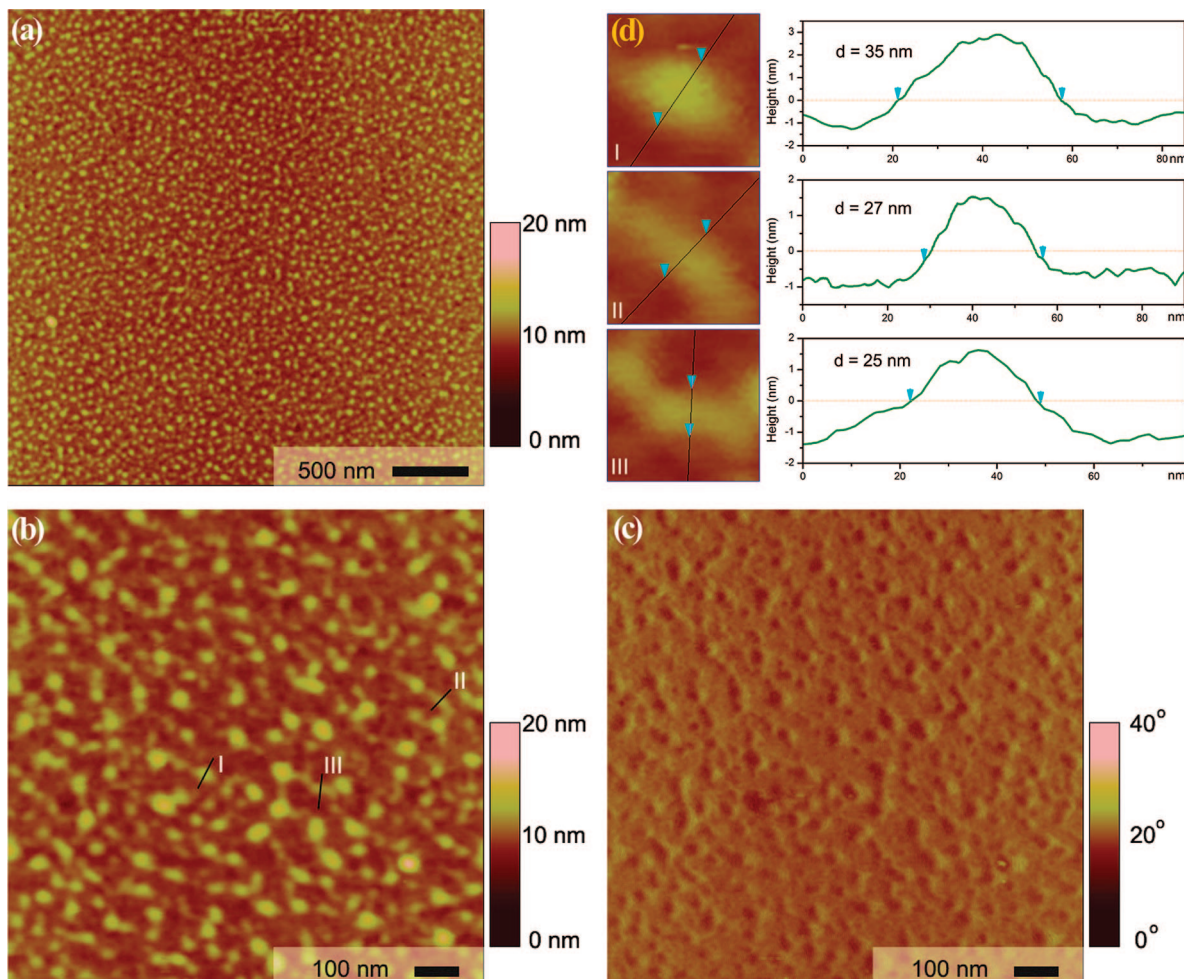


Figure 1. Representative tapping-mode AFM images of the interface of PBTDT thin film without annealing. (a) AFM topography (image size: $3.2 \times 3.2 \mu\text{m}$). (b and c) AFM topography and phase image (image size: $1.1 \times 1.1 \mu\text{m}$). (d) Cross-section taken across the rod-like nanoparticles marked I, II and III in part b.

boundaries between the rod-like nanoparticles.²⁴ Even though a number of approaches through forming fibrillar/whisker or nanorod structures^{22,24–29} were used to explore the microstructure for understanding the effect of microstructure on the mobility enhancement, the characterizations were not directly carried on the interface layer where most of the charge carriers transferred and might not reflect the real mechanism responsible for the improved transistor performance. The results discussed above indicate that this work reveals reliable and important information for fundamentals to explain the effects of processing conditions such as solvent and thermal treatment that are known to improve the OTFT performance.

3.2. HRTEM Characterizations. Direct observation and analysis of the microstructure in the interface for detail crystallinity and orientation within domains and boundaries with atomic resolution have never been achieved although it is very important to study the fundamentals of the charge carrier transport in the interface of the organic thin film. HRTEM is an optimal tool to explore the detail microstructure within the polymer nanocrystalline and disordered boundaries with its low-dose mode which can efficiently reduce the structure damage on the polymer.^{44,49} To conduct such a study, it is critical to prepare a free-standing thin film with thickness less than 100 nm, and the interface surface of the film should be exposed upward where the orientation of the lamellar could be highly consistent with the edge-on orientation,⁷ i.e., the lamellar plane (face (010)) is parallel to the electron beam direction for

HRTEM characterizations. In this work, functionalized self-assembled monolayers (SAMs) of OTS-8 are used to direct the ordering of lamellar stacks of polymers in such a way that the π - π stacking is oriented parallel to the modified surface (as shown by the schematic in Figure 4), an edge-on orientation.^{18,39,41,50,51} The freestanding interface film sample could be easily delaminated using a floating off process^{41–44} with insignificant damage of the interface layer.

Figure 5 shows the typical HRTEM images and corresponding selective area electron diffraction (SAED) patterns of PBTDT thin films delaminated from mica without and with annealing, in which the spin-coating thin film without thermal treatment (Figure 5a) illustrate randomly distributed PBTDT nanocrystals with size of about 15 nm in diameter. This is consistent with the length of the polymer mainchain estimated from molecular weight ($M_n = 7900$) but a little smaller than that measured in Figure 1d, which is possibly due to the overestimated width in AFM measurements from the stickiness between AFM tips and polymer surface. However, the morphology can be considered in good agreement with the AFM observations, i.e., most of the nanocrystals are separately distributed with amorphous intersection area except that few of them are overlapped. It is reasonable that overlapping of misoriented grains and intersecting features might appear in the images since HRTEM image is in essence a projection from a three-dimensional structure. Both the HRTEM image and SAED pattern identify the existence of (020) plane (or called edge-on orientation^{50,51}) with

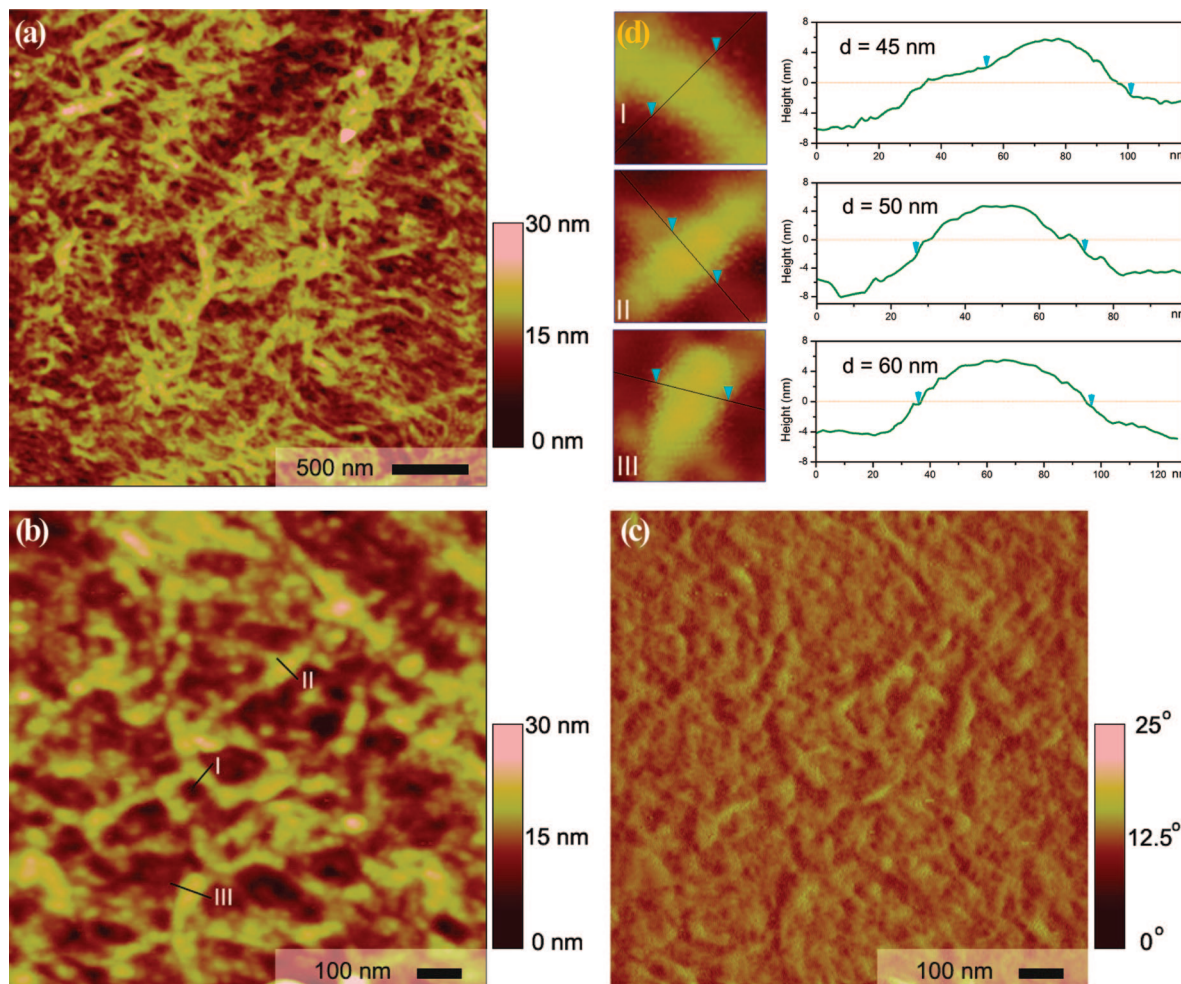


Figure 2. Representative tapping-mode AFM images of the interface of PBTDT thin film after annealing. (a) AFM topography (image size: $3.2 \times 3.2 \mu\text{m}$). (b and c) AFM topography and phase image (image size: $1.1 \times 1.1 \mu\text{m}$). (d) Cross-section taken across the fibers marked I, II and III in part b.

$\pi-\pi$ stacking distance of 0.38 nm. Because of the limitation of SAED to obtain lattice information from smaller size nanocrystals, fast Fourier transformation (FFT) was conducted from the square region consisting of two nanocrystals. The FFT patterns in parts b and c of Figure 5 not only reveals the crystalline structure with stacking (020) lamellae but also clearly depicts two different orientations of these two nanocrystals with a boundary tilt angle of 56°. Figure 5d shows the typical highly crystalline structure of PBTDT thin film after annealing. Obviously, highly ordered lamellar structure in much larger area (several tens of nanometers) was formed with lattice separation of about 0.33 nm. Few lattice curvature or dislocations within the grains can be observed and the grains are closely interconnected with less amorphous structure in the boundary area. The inset SAED pattern in Figure 5d can be indexed as (020) reflection. In comparison to that of PBTDT thin film without annealing, SAED result shows that the $\pi-\pi$ stacking distance shrinks to about 0.33 nm after annealing. The $\pi-\pi$ stacking distance is slightly smaller than normal, indicating a more coplanar backbone structure in the annealed PBTDT nanocrystals. Compared with SAED in which electrons penetrate a relative large area of the sample, the use of FFT can help to obtain structure information from single-crystalline grain. The rectangular symmetry of the patterned spots in Figure 5e implies that the PBTDT grain might be orthorhombic structure proposed hereinafter and the reflections can be indexed as $(0h)$ and $(0h\pm 3)$, as shown in Figure 5f.

Obviously, thermal treatment results in significant lattice structure changes according to above HRTEM characterizations. Considering the orthorhombic unit cell proposed by Winokur et al.^{52,53} and a *syn-anti* conformation around the thiophene-dithieno[3,2-*b*;2',3'-*d*]thiophene bonds confirmed by Frey et al.,⁵⁴ we proposed that the unit cell of PBTDT after annealing is orthorhombic with $a = d_{100} = 20.9 \text{ \AA}$, $b = 2d_{020} = 6.6 \text{ \AA}$, $c = 15.1 \text{ \AA}$, $\alpha = \beta = \gamma = 90^\circ$ based on previous XRD data⁴⁰ (See Figure S5 and structure discussion in Supporting Information). Figure 6 shows HRTEM image of PBTDT mainchains at an atomic scale, accompanied with the simulated image (Figure 6b) and the schematic illustration (Figure 6c) based on the proposed atomic model. It was found that contrast along [001] in simulated image show reasonable qualitative matching with the experimental image. This indicates that not only the proposed lattice parameters are reasonable for PBTDT nanocrystals but also the indexed SAED and FFT patterns discussed above are self-consistent and credible.

The result here directly images molecular arrangement inside the domains and near grain boundaries at atomic scale from the interface layer of organic thin film, which not only reveals the fine structures inside crystalline domains and at amorphous boundaries but also shows significant lattice structure changes and the enhancement of the overall crystallinity in the samples after annealing. By a thorough analysis of the HRTEM images, SAED and FFT patterns, it can be concluded that there are three main structural variations after annealing: the increased domain

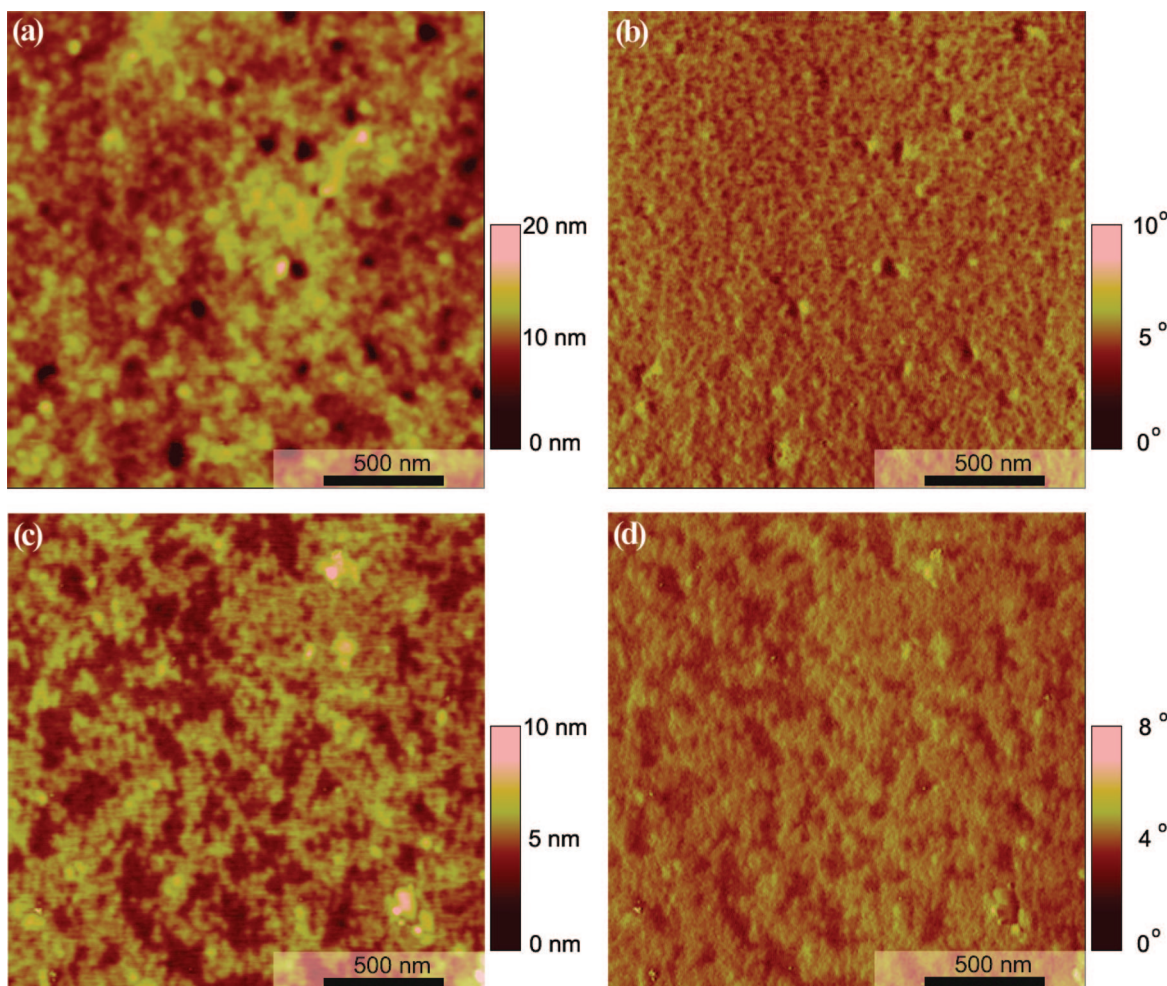


Figure 3. (a) AFM topography and (b) phase image from top surface of PBTDT thin film without annealing (image size: $2.0 \times 2.0 \mu\text{m}$; root-mean-square (rms) roughness: 15.3 \AA). (c) AFM topography and (d) phase image from top surface of PBTDT thin film after annealing (image size: $2.0 \times 2.0 \mu\text{m}$; root-mean-square (rms) roughness: 7.6 \AA).

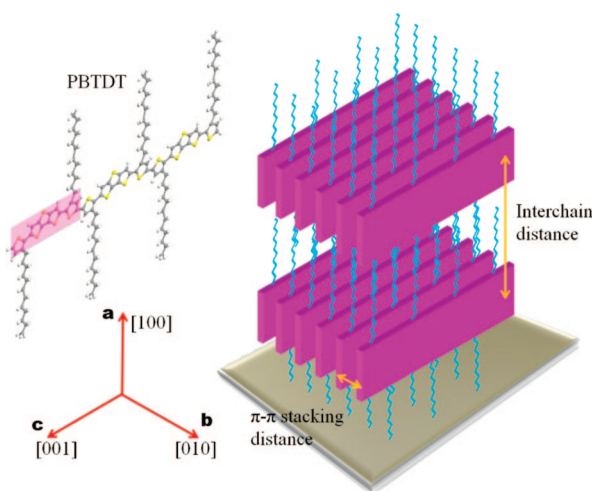


Figure 4. Schematic representation of the crystalline lamellae of PBTDT oriented on OTS-8 modified substrate.

size from merging of domains, formation of a more coplanar backbone and reduction of π - π stacking distance, and reduction of disorders in grain boundary. The anisotropy of PBTDT crystals limits charge transport to two crystal directions: [010] and [001], while the insulating alkyl chain preventing charge transport in the [100] direction. Considering charge transport in a single crystalline domain, there is no doubt that larger

domain size can greatly benefit the charge transport because the transport along the conjugated segments of the polymer backbone (along [001] direction) is faster than interchain hopping between adjacent chains (along [010] direction).²⁶ The grain boundary is another key factor that determines the charge transport in whole thin film and will be discussed in detailed latter.

Theoretically, the charge-transport properties of an organic transistor strongly depend on the extent of the electronic coupling,^{46,55} which decays exponentially with intermolecular distance because of the exponential decay of intermolecular π -atomic orbital overlap.^{46,55} In a real case, the transfer integrals strongly rely on the mode of packing, molecular displacements and intermolecular distance. HRTEM results show that the intermolecular distance (π - π stacking distance) is reduced from 0.38 to 0.33 nm. This could greatly enhance the interchain transport efficiency of charge carriers since the electronic couplings can increase by as many as a factor of 3–4 between 0.33 and 0.4 nm.⁴⁶ Thus, high efficient interchain transport could be one of the key factors that are responsible for the improved charge transfer inside domains after annealing process of thin film.

3.3. Grain Boundaries. Figure 7 shows the typical grain boundaries observed from the PBTDT thin film without and with annealing. The boundaries between two grains and among three grains in the interface of spin-coating PBTDT thin film

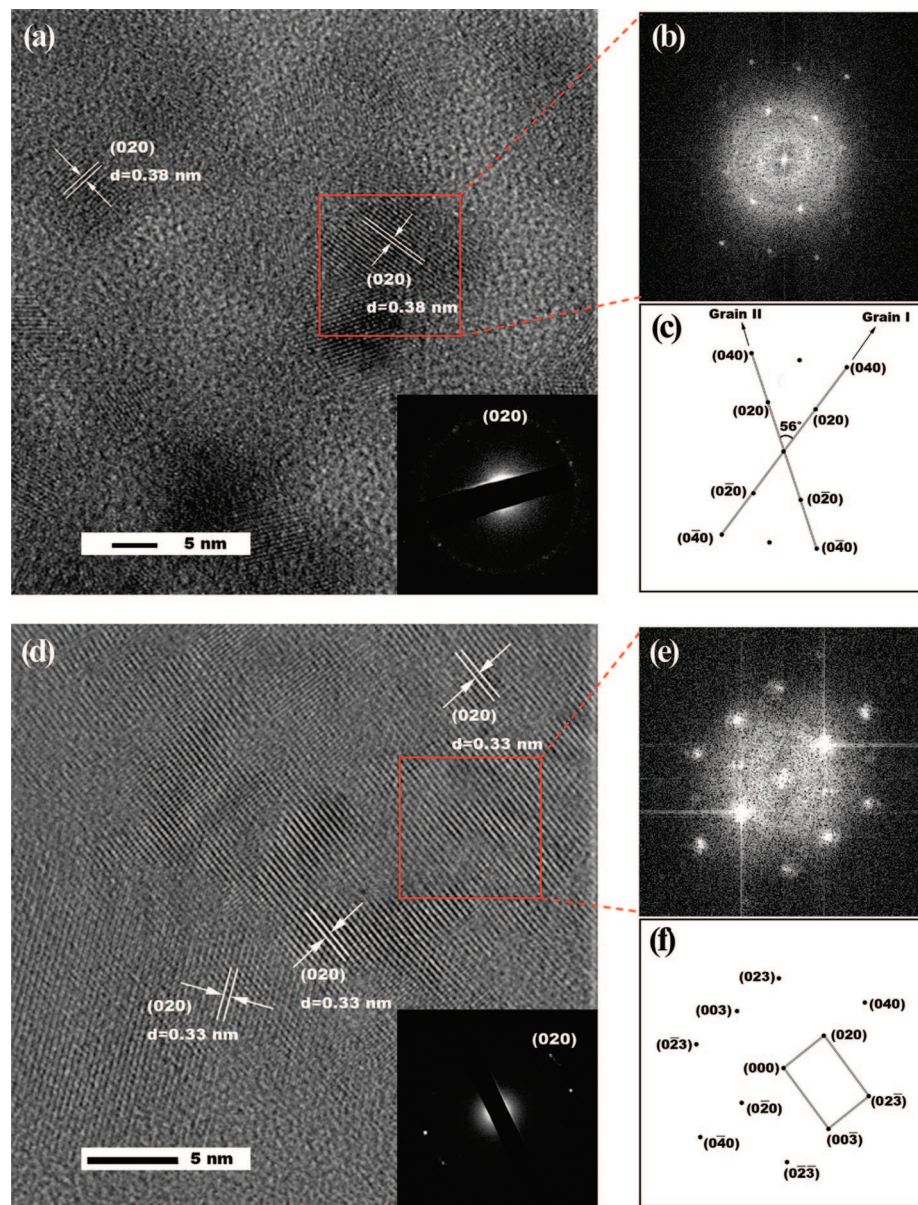


Figure 5. (a) HRTEM image of the interface of PBTDT thin film without annealing and corresponding SAED ring pattern (inset). (b) FFT pattern conducted from the square region containing two grains in part a and the planes are indexed in part c. (d) HRTEM image of the interface of PBTDT thin film after annealing and corresponding SAED ring pattern (inset). (e) FFT pattern conducted from the square region in part d and the planes are indexed in part f.

fabricated by us are clearly discerned in Figure 7, parts a and b, which reveals that the lamellar structure is rigid within grains but the mainchains are curved or disturbed in the surface or amorphous intergrain zones. According to the relative orientations of these grains, they can be classified into a typical side-to-side grain boundary¹⁵ with large boundary tilt angles ($\theta = 56^\circ, 43^\circ, 72^\circ$, and 69°). The side-to-side grains demonstrated in Figure 7a have the possibility of a reasonably smooth connection in some regions. However, in the annealed thin film, the amorphous region between two grains can hardly be seen (Figure 7c, d); instead, the grain boundaries illustrate typical end-to-end connection with some interpenetration of the chains along with considerable disorder. Relative small boundary tilt angles $\theta = 56^\circ$ and 55° can be obtained.

Grain boundaries are considered as regions where symmetry and molecular connectivity are disrupted and the molecular connections and interactions remain intact through structural relaxations.⁵⁶ It is known that intermolecular charge hopping

across grain boundaries, or through disordered domains, is not as efficient as within ordered domains, and thus the molecular arrangement near grain boundaries can strongly affect the charge mobility in an organic semiconducting thin film. However, the structures in the grain boundaries at the interface have not been conducted before due to the limitation of conventional structural characterization methods such as XRD and NEXAFS. Recently, lattice defects such as grain boundaries and dislocations in pentacene nanocrystals were imaged by use of low-dose HRTEM,⁴⁴ but the sample prepared by mechanical disruption of the neat powder cannot represent the thin film in a real device. The results in Figure 7 demonstrate the microstructural variations of grain boundaries in the interface of a thin organic semiconducting film for the first time (More HRTEM images on grain boundary are shown in Figure S6 in Supporting Information).

The microstructural variations in the boundaries revealed in Figure 7 could provide important and solid support to fundamentally explain the improvement of charge transport through

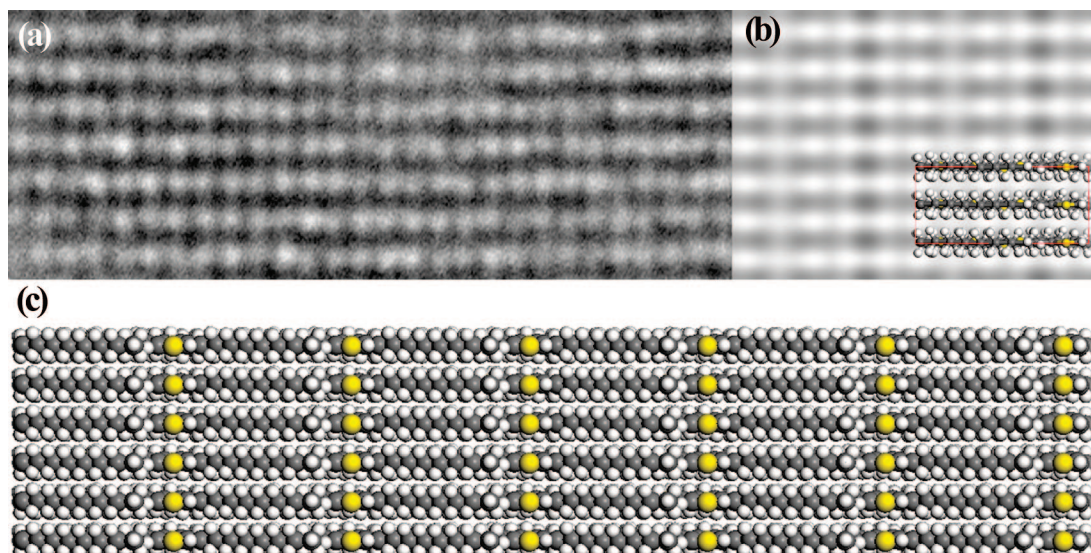


Figure 6. (a) HRTEM image of main chains from the interface of highly crystalline PBTDT thin film after annealing. (b) Simulated image from a $10 \times 4 \times 4$ supercell projected in [100] direction, only 4 unit cells are shown, of which one unit cell is shown with atomic model. (c) Schematic atom model of the main chain cleaved in (100) face (C, dark balls; S, yellow balls; H, white balls).

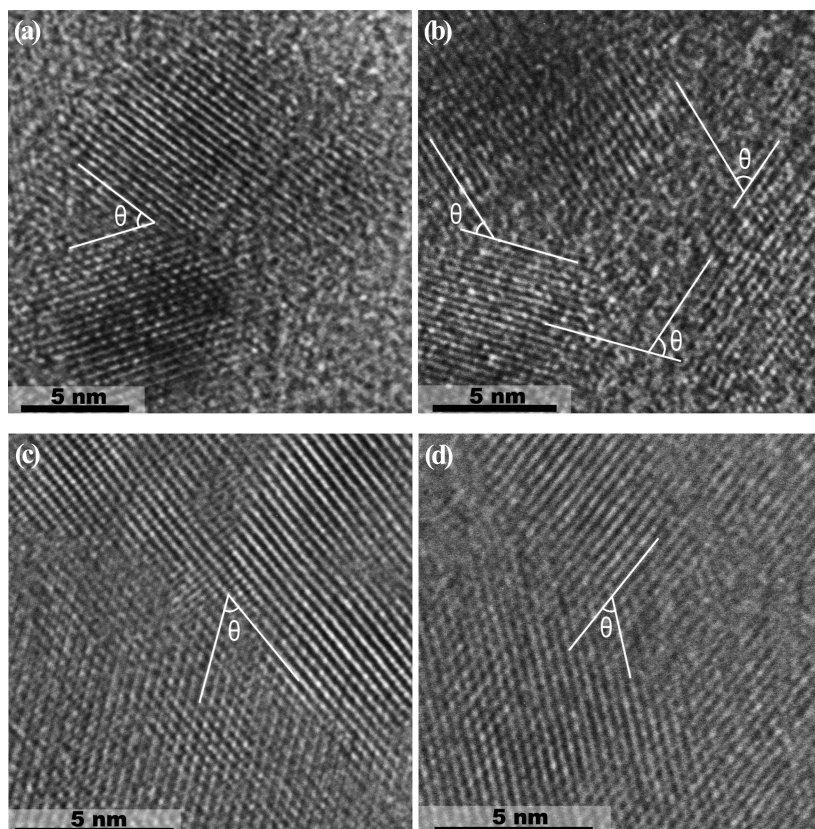


Figure 7. HRTEM images of typical grain boundaries from the interface of PBTDT thin film: (a and b) without annealing; (c and d) after annealing. Part a is magnified from Figure 5a, and part c is magnified from Figure 5d. Boundary tilt angle: (a) $\theta = 56^\circ$; (b) $\theta = 43^\circ$ (left), 72° (center) and 69° (right); (c) $\theta = 56^\circ$; (d) $\theta = 55^\circ$.

the annealing process. Obviously, the annealing process reduces the amorphous intergrain zones, resulting in fewer insulating grain boundaries in the plane of charge transport. Further, the mainchains are unbent and even are interpenetrated into neighboring grains after annealing, leading to stronger electronic overlap along high-mobility directions between neighboring grains.³⁹ In addition, the highly misoriented grain boundaries with poor electronic overlap are reduced and small-angle boundaries with end-to-end connections are formed after the

post-thermal treatment. Transport properties of charge carriers can be significantly influenced by the boundary tilt angles, of which the smallest angle is the most favorable transport direction since the grain boundaries are not isotropic.^{57,58} Our work also demonstrates angle reduction after annealing. Thus, all the structural variations render great evidence to scientific insights to the performance improvement of the OTFT after annealing. It is hard to give an accurate quantitative analysis of the microstructural variations after annealing due to the inhomogeneity of the film.

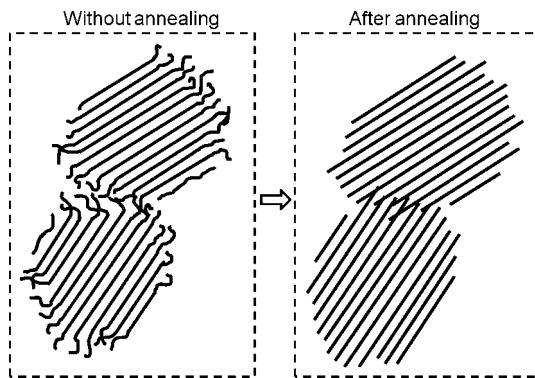


Figure 8. Schematic representation shows the microstructural variations around the grain boundary induced by annealing. Each line represents one mainchain of semicrystalline polymer projected from [100] direction.

genetics of grain boundaries. However, based on our systematical HRTEM observations, a schematic model was proposed in Figure 8 to qualitatively describe the microstructural variations around the grain boundaries induced by annealing. As the backbone of PBTDT is quite stiff, chain folding was neglected in the model according to polymer crystallization.⁵⁹ On the basis of the experimental results and theoretical analysis, it is believed that the distinctive microstructural variations in the boundary area are responsible for the improved transistor performance after annealing the PBTDT thin film.

4. Conclusions

Microstructural variations of crystalline domains and grain boundaries in the buried interface of an organic semiconductor thin film by AFM and HRTEM are directly observed. The experimental results and theoretical analysis through a newly synthesized polymer PBTDT as an example reveal that annealing of an organic semiconducting thin film induces distinctive microstructural variations at the interface that are responsible for the enhanced performance of OTFT. An annealing-induced network nanostructure of crystalline nanofibers at the interface shows distinct feature from the outside surface of the film, which facilitates interfiber charge transport at nanometer scale. The fine structure revealed in this work demonstrates annealing induced larger domains from merging and growing, enhanced crystallinity of domains, reduced $\pi-\pi$ stacking distance, reduced disorders in the grain boundaries and small-angle boundaries with end-to-end connections, which can significantly enhance charge hopping efficiency between mainchains and grains at a molecule scale. This is likely to represent a general feature of semicrystalline polymer thin films after post thermal treatment. The observations render important information for deep scientific insights of the OTFT performance improvement through a process approach, and may possibly guide us to better engineer high-quality polymer thin films for OTFTs after fully understanding the effect of microstructural variations on the performance improvement.

Acknowledgment. This work was financially supported by Singapore A*STAR Grant No: 052 117 0031.

Supporting Information Available: Text discussing and figures showing transistor properties, optical microscopy, optical measurements, AFM images of mica, XRD results and structure, and more HRTEM images on grain boundary. This material is available free of charge via the Internet at <http://pubs.acs.org>.

References and Notes

- (1) Friend, R. H.; Gymer, R. W.; Holmes, A. B.; Burroughes, J. H.; Marks, R. N.; Taliani, C.; Bradley, D. D. C.; Dos Santos, D. A.; Bredas, J. L.; Logdlund, M.; Salaneck, W. R. *Nature* **1999**, *397*, 121.
- (2) Heeger, A. J. *Angew. Chem., Int. Ed.* **2001**, *40*, 2591.
- (3) Tessler, N.; Medvedev, V.; Kazes, M.; Kan, S. H.; Banin, U. *Science* **2002**, *295*, 1506.
- (4) Huynh, W. U.; Dittmer, J. J.; Alivisatos, A. P. *Science* **2002**, *295*, 2425.
- (5) Brabec, C. J.; Sariciftci, N. S.; Hummelen, J. C. *Adv. Funct. Mater.* **2001**, *11*, 15.
- (6) Burroughes, J. H.; Jones, C. A.; Friend, R. H. *Nature* **1988**, *335*, 137.
- (7) Sirringhaus, H.; Brown, P. J.; Friend, R. H.; Nielsen, M. M.; Bechgaard, K.; Langeveld-Voss, B. M. W.; Spiering, A. J. H.; Janssen, R. A. J.; Meijer, E. W.; Herwig, P.; de Leeuw, D. M. *Nature* **1999**, *401*, 685.
- (8) Sirringhaus, H. *Adv. Mater.* **2005**, *17*, 2411.
- (9) Sirringhaus, H.; Tessler, N.; Friend, R. H. *Science* **1998**, *280*, 1741.
- (10) Ong, B. S.; Wu, Y. L.; Liu, P.; Gardner, S. *J. Am. Chem. Soc.* **2004**, *126*, 3378.
- (11) Ong, B. S.; Wu, Y. L.; Liu, P.; Gardner, S. *Adv. Mater.* **2005**, *17*, 1141.
- (12) McCulloch, I.; Heeney, M.; Bailey, C.; Genevicius, K.; Macdonald, I.; Shkunov, M.; Sparrowe, D.; Tierney, S.; Wagner, R.; Zhang, W. M.; Chabinyc, M. L.; Kline, R. J.; McGehee, M. D.; Toney, M. F. *Nat. Mater.* **2006**, *5*, 328.
- (13) Sirringhaus, H.; Kawase, T.; Friend, R. H.; Shimoda, T.; Inbasekaran, M.; Wu, W.; Woo, E. P. *Science* **2000**, *290*, 2123.
- (14) Vissenberg, M.; Matters, M. *Phys. Rev. B* **1998**, *57*, 12964.
- (15) Street, R. A.; Northrup, J. E.; Salleo, A. *Phys. Rev. B* **2005**, *71*, 165202.
- (16) Bao, Z.; Dodabalapur, A.; Lovinger, J. A. *Appl. Phys. Lett.* **1996**, *69*, 4108.
- (17) Lu, G. H.; Li, L. G.; Yang, X. N. *Adv. Mater.* **2007**, *19*, 3594.
- (18) Salleo, A.; Chabinyc, M. L.; Yang, M. S.; Street, R. A. *Appl. Phys. Lett.* **2002**, *81*, 4383.
- (19) Kim, D. H.; Park, Y. D.; Jang, Y. S.; Yang, H. C.; Kim, Y. H.; Han, J. I.; Moon, D. G.; Park, S. J.; Chang, T. Y.; Chang, C. W.; Joo, M. K.; Ryu, C. Y.; Cho, K. W. *Adv. Funct. Mater.* **2005**, *15*, 77.
- (20) Sirringhaus, H.; Wilson, R. J.; Friend, R. H.; Inbasekaran, M.; Wu, W.; Woo, E. P.; Grell, M.; Bradley, D. D. C. *Appl. Phys. Lett.* **2000**, *77*, 406.
- (21) Savenije, T. J.; Kroze, J. E.; Yang, X. N.; Loos, J. *Adv. Funct. Mater.* **2005**, *15*, 1260.
- (22) Kline, R. J.; McGehee, M. D.; Kadnikova, E. N.; Liu, J. S.; Frechet, J. M. J. *Adv. Mater.* **2003**, *15*, 1519.
- (23) Salleo, A. *Mater. Today* **2007**, *10*, 38.
- (24) Kline, R. J.; McGehee, M. D.; Kadnikova, E. N.; Liu, J. S.; Frechet, J. M. J.; Toney, M. F. *Macromolecules* **2005**, *38*, 3312.
- (25) Yang, H. C.; Shin, T. J.; Yang, L.; Cho, K.; Ryu, C. Y.; Bao, Z. N. *Adv. Funct. Mater.* **2005**, *15*, 671.
- (26) Zhang, R.; Li, B.; Iovu, M. C.; Jeffries-El, M.; Sauve, G.; Cooper, J.; Jia, S. J.; Tristram-Nagle, S.; Smilgies, D. M.; Lambeth, D. N.; McCullough, R. D.; Kowalewski, T. *J. Am. Chem. Soc.* **2006**, *128*, 3480.
- (27) Zen, A.; Pflaum, J.; Hirschmann, S.; Zhuang, W.; Jaiser, F.; Asawapirom, U.; Rabe, J. P.; Scherf, U.; Neher, D. *Adv. Funct. Mater.* **2004**, *14*, 757.
- (28) Zen, A.; Saphiannikova, M.; Neher, D.; Grenzer, J.; Grigorian, S.; Pietsch, U.; Asawapirom, U.; Janietz, S.; Scherf, U.; Lieberwirth, I.; Wegner, G. *Macromolecules* **2006**, *39*, 2162.
- (29) Ihn, K. J.; Moulton, J.; Smith, P. *J. Polym. Sci., Part B: Polym. Phys.* **1993**, *31*, 735.
- (30) Ong, B. S.; Wu, Y. L.; Liu, P.; Gardner, S. *Adv. Mater.* **2005**, *17*, 1141.
- (31) Pan, H. L.; Li, Y. N.; Wu, Y. L.; Liu, P.; Ong, B. S.; Zhu, S. P.; Xu, G. *J. Am. Chem. Soc.* **2007**, *129*, 4112.
- (32) Fritz, S. E.; Martin, S. M.; Frisbie, C. D.; Ward, M. D.; Toney, M. F. *J. Am. Chem. Soc.* **2004**, *126*, 4084.
- (33) Jun, Y. S.; Zhu, X. Y. *J. Am. Chem. Soc.* **2004**, *126*, 13224.
- (34) Kaake, L. G.; Zou, Y.; Panzer, M. J.; Frisbie, C. D.; Zhu, X. Y. *J. Am. Chem. Soc.* **2007**, *129*, 7824.
- (35) Lefenfeldt, M.; Baumert, J.; Sloutskin, E.; Kuzmenko, I.; Pershan, P.; Deutscher, M.; Nuckolls, C.; Ocko, B. M. *PNAS* **2006**, *103*, 2541.
- (36) Ho, P. K. H.; Chua, L. L.; Dipankar, M.; Gao, X. Y.; Qi, D. C.; Wee, A. T. S.; Chang, J. F.; Friend, R. H. *Adv. Mater.* **2007**, *19*, 215.
- (37) Yuan, Q.; Mannsfeld, S. C. B.; Tang, M. L.; Toney, M. F.; Luening, J.; Bao, Z. A. *J. Am. Chem. Soc.* **2008**, *130*, 3502.
- (38) DeLongchamp, D. M.; Kline, R. J.; Lin, E. K.; Fischer, D. A.; Richter, L. J.; Lucas, L. A.; Heeney, M.; McCulloch, I.; Northrup, J. E. *Adv. Mater.* **2007**, *19*, 833.
- (39) Kline, R. J.; McGehee, M. D.; Toney, M. F. *Nat. Mater.* **2006**, *5*, 222.

- (40) Li, J.; Qin, F.; Li, C. M.; Bao, Q. L.; Chan-Park, M. B.; Zhang, W.; Qin, J.; Ong, B. S. *Chem. Mater.* **2008**, *20*, 2057.
- (41) Zhao, N.; Botton, G. A.; Zhu, S. P.; Duft, A.; Ong, B. S.; Wu, Y. L.; Liu, P. *Macromol.* **2004**, *37*, 8307.
- (42) Lovinger, A. J.; Davis, D. D.; Dodabalapur, A.; Katz, H. E.; Torsi, L. *Macromolecules* **1996**, *29*, 4952.
- (43) Gonzalez-Ronda, L.; Martin, D. C. *Macromolecules* **2004**, *37*, 2872.
- (44) Drummy, L. F.; Kubel, C.; Lee, D.; White, A.; Martin, D. C. *Adv. Mater.* **2002**, *14*, 54.
- (45) Stadelmann, P. A. *Ultramicroscopy* **1987**, *21*, 131.
- (46) Coropceanu, V.; Cornil, J.; da Silva, D. A.; Olivier, Y.; Silbey, R.; Bredas, J. L. *Chem. Rev.* **2007**, *107*, 926.
- (47) Zaumseil, J.; Sirringhaus, H. *Chem. Rev.* **2007**, *107*, 1296.
- (48) Chang, J. F.; Clark, J.; Zhao, N.; Sirringhaus, H.; Breiby, D. W.; Andreassen, J. W.; Nielsen, M. M.; Giles, M.; Heeney, M.; McCulloch, I. *Phys. Rev. B* **2006**, *74*.
- (49) Martin, D. C.; Thomas, E. L. *Polymer* **1995**, *36*, 1743.
- (50) Brinkmann, M.; Wittmann, J. C. *Adv. Mater.* **2006**, *18*, 860.
- (51) Brinkmann, M.; Rannou, P. *Adv. Funct. Mater.* **2007**, *17*, 101.
- (52) Prosa, T. J.; Winokur, M. J.; Moulton, J.; Smith, P.; Heeger, A. J. *Macromol.* **1992**, *25*, 4364.
- (53) Tashiro, K.; Kobayashi, M.; Kawai, T.; Yoshino, K. *Polymer* **1997**, *38*, 2867.
- (54) Frey, J.; Bond, A. D.; Holmes, A. B. *Chem. Commun.* **2002**, 2424.
- (55) Bredas, J. L.; Calbert, J. P.; da Silva, D. A.; Cornil, J. *PNAS* **2002**, *99*, 5804.
- (56) Kubel, C.; Gonzalez-Ronda, L.; Drummy, L. F.; Martin, D. C. *J. Phys. Org. Chem.* **2000**, *13*, 816.
- (57) Chwang, A. B.; Frisbie, C. D. *J. Phys. Chem. B* **2000**, *104*, 12202.
- (58) Liao, J.; Martin, D. C. *Macromol.* **1996**, *29*, 568.
- (59) Ungar, G.; Zeng, K. B. *Chem. Rev.* **2001**, *101*, 4157.

JP804988H